Nanomanipulation and Nanotribology of Nanoparticles and Nanotubes Using Atomic Force Microscopy

10

Dave Maharaj and Bharat Bhushan

Keywords
Nano-objects • Nanomanipulation • Nanotribology • Friction • Wear

Introduction

Nanoparticles and nanotubes have been investigated for applications that require controlled manipulation and targeting in biomedicine and the oil industry and tribology on the macro- to nanoscale. Knowledge of interfacial friction and wear is important for determining their suitability for various applications.

In controlled manipulation and targeting, applications include but are not limited to use in targeted drug delivery and chemical sensors in the identification of oil, removal of contaminants, and enhanced oil recovery (EOR). Au, Fe_2O_3, polymer, and Si nano-objects have been studied in targeted drug delivery [12, 14, 19, 31]. Figure 10.1a shows a nanoparticle loaded with a therapeutic drug and functionalized with a biomolecule (ligand), which selectively attaches to receptors in a cancer cell. The drug is then released as the nanoparticle diffuses into the diseased cell resulting in cell death. In applications requiring chemical sensors, nanoparticles and nanotubes including oxidized carbon black coated with oil-detecting agents and composites of collagen and superparamagnetic iron oxide nanoparticles have been used [2, 28, 36, 41]. Figure 10.1b shows an example of nanoparticles being used as a chemical sensor in oil detection. Oxidized carbon black nanoparticles with a polyvinyl alcohol shell are coated with an oil-detecting agent, 2,2′,5,5′-tetrachlorobiphenyl (PCB). The release of this agent on contact with

D. Maharaj • B. Bhushan (✉)
Nanoprobe Laboratory for Bio- & Nanotechnology and Biomimetics (NLBB), The Ohio State University, Columbus, OH, USA
e-mail: Bhushan.2@osu.edu

B. Bhushan et al. (eds.), *Handbook of Nanomaterials Properties*,
DOI 10.1007/978-3-642-31107-9_18,

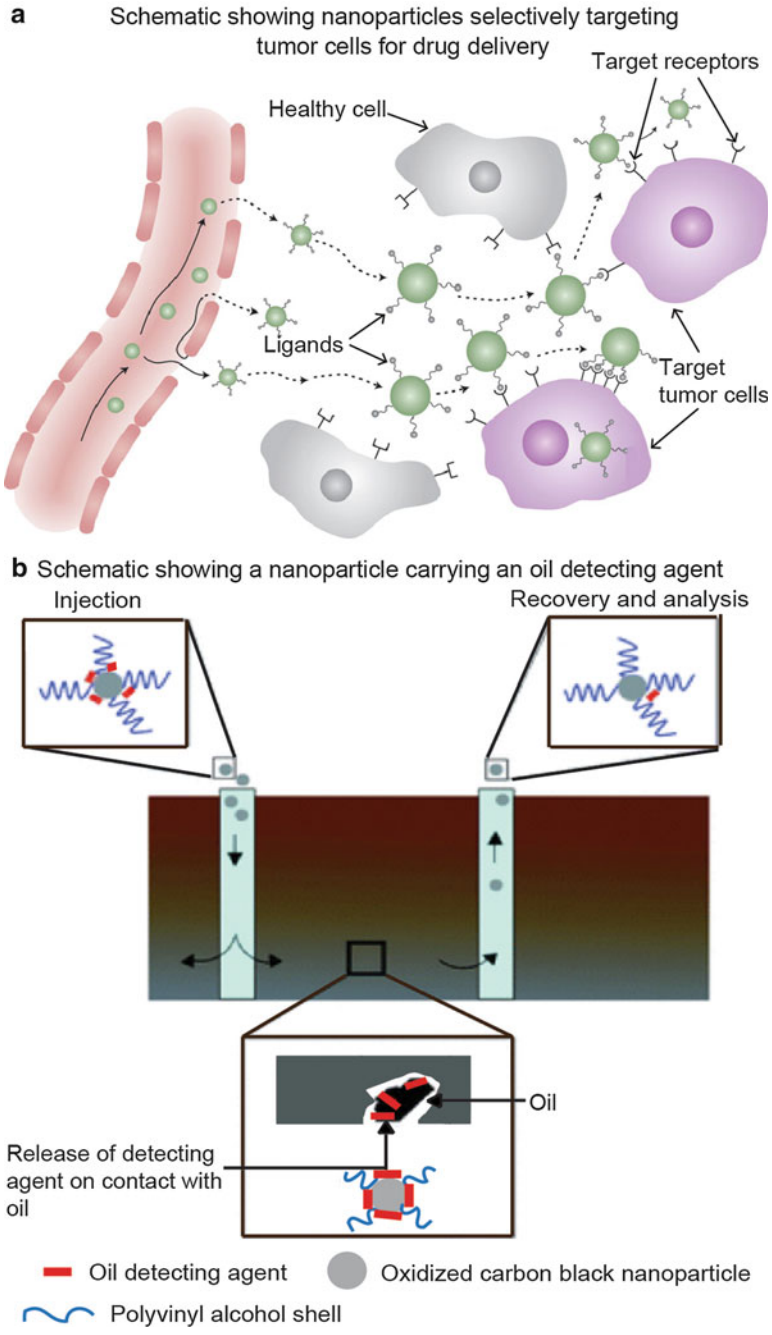

Fig. 10.1 Schematics (**a**) of a drug carrying nanoparticles targeting cancer cells and releasing their therapeutic payload resulting in death of the cancer cell [19] (**b**) showing the process of oil

hydrocarbons is used as an indication of the presence of oil, on nanoparticle recovery [2]. In both of these applications, low friction in liquid medium is of interest. In manipulation studies with an AFM under dry conditions, several groups have demonstrated the contact area and relative humidity dependence of friction force [11, 25, 29, 30, 35]. Studies carried out in liquid environments have shown reductions in friction force [25–27].

For tribological applications on the micro-/nanoscale, increasing the lifetime and efficiency of individual components of systems is crucial to the commercialization of micro-/nanoelectromechanical systems (MEMS/NEMS) [3]. Adhesive and friction forces, which are surface area dependent, become more significant as surface to volume ratio increases. With MEMS/NEMS devices, the initial start-up forces and torques needed become high, which can hinder device operation and reliability [4]. The choice of a suitable lubricant on these scales becomes crucial.

Nanoparticles including Au, carbon nanohorns (CNH), Fe_2O_3, Sb, MoS_2, and WS_2; nanorods including ZnS, ZnO, and $AgVO_3$; and nanotubes including MoS_2, WS_2, and carbon nanotubes (CNT) have been studied in tribological applications on the macro- to nanoscale. Studies have been carried out in dry conditions on the macroscale [5, 25–27, 32, 39], microscale using a surface force apparatus (SFA) [43, 45], and the nanoscale using an AFM [11, 18, 22, 24–27, 29, 30, 35, 38, 40]. In liquid conditions studies have also been carried out on the macroscale [5, 9, 10, 16, 17, 20, 21, 25–27, 33], microscale, using an SFA [1, 15], and nanoscale using an AFM [25–27, 34].

In nanotribological studies using an AFM, reductions in friction and wear were observed when Au, silica, and CNH nanoparticles and MoS_2 and WS_2 nanotubes were used as lubricants in dry conditions [25–27, 30]. Further reductions in friction and wear were obtained when nano-objects were submerged in water, dodecane, and glycerol [25–27]. Reductions in friction and wear as a result of the presence of nano-objects are believed to occur through rolling, sliding, and dragging of nano-objects as depicted in Fig. 10.2a–c with CNH nanoparticles as an example. Nano-objects made of lamellar materials can also reduce friction and wear through the exfoliation and tribofilm formation as shown in Fig. 10.2d, e. In the case of CNH nanoparticles, the additional roughness provided by the nanohorns can further reduce the contact area of the nanoparticles. This together with their low meniscus force contribution to adhesion further enhances the ability to reduce friction and wear [27].

To characterize friction forces and understand the mechanism of friction and wear reduction of nano-objects, nanoscale studies have been carried in both single- and multiple-nano-object contact using an AFM. In single-nano-object contact studies, nano-objects are pushed laterally using an AFM tip and provide

Fig. 10.1 (continued) detection with nanoparticles. The carbon black nanoparticles are coated with an oil-detecting agent. After injection into the ground, the agent is released on contact with hydrocarbons and this is used as an indication of the presence of oil on recovery and analysis of the nanoparticle [2]

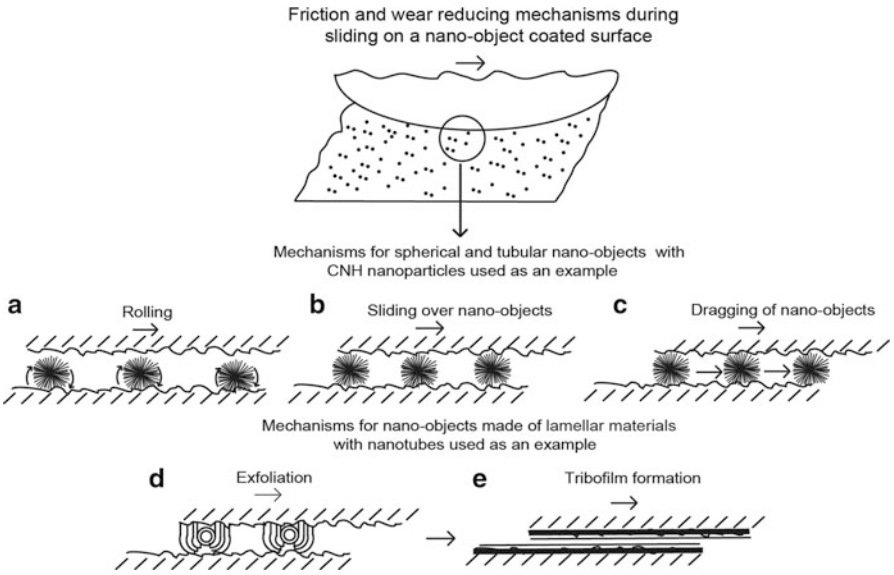

Fig. 10.2 Schematic of friction and wear reducing mechanism of nano-object-coated surface by (**a**) rolling, (**b**) sliding over nano-objects, (**c**) dragging of nano-objects, (**d**) exfoliation, and (**e**) tribofilm formation. Carbon nanohorns (*CNH*) are used as an example for mechanisms (**a**) through (**c**), and WS_2 and MoS_2 nanotubes are used as an example for mechanisms (**d**) through (**e**) [27]

understanding of the nature of the friction mechanism. Multiple-nano-object contact studies simulate the ensuing contacts experienced when nano-objects are introduced for the purpose of friction and wear reduction.

This chapter will present an overview of friction and wear of Au and CNH nanoparticles and MoS_2 and WS_2 nanotubes in dry and submerged-in-liquid environments.

Single- and Multiple-Nano-object Contact

In this section, results from experiments in single- and multiple-nano-object contact are presented for dry conditions and submerged-in-liquid conditions for water, dodecane, and glycerol [25–27]. In single-nano-object contact, as shown in Fig. 10.3a as an example, a sharp tip with a nominal radius of 15 nm was used to push the nano-object laterally. In multiple-nano-object contact as shown in Fig. 10.3b as an example, a glass sphere attached to an AFM tip was used to slide over several nano-objects [27]. The friction forces are presented for Au 30, Au 90, and CNH nanoparticles and MoS_2 and WS_2 nanotubes. In addition, wear data on the nanoscale with and without addition of nanoparticles and nanotubes are also presented. Morphological characterization of the nano-objects and wear scars are also shown.

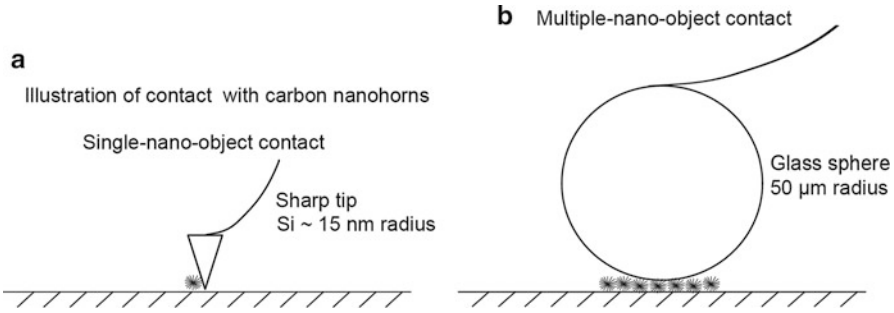

Fig. 10.3 Schematics of (**a**) a sharp tip pushing a nano-object in single-nano-object contact and (**b**) a glass sphere sliding over several nano-objects in multiple-nano-object contact [27]

Single-Nano-object Contact: Lateral Manipulation of Nano-objects over a Silicon Substrate in Dry and Submerged-in-Liquid Environments

For single-nano-object contact under dry conditions, a sharp tip was used to push the nano-objects in the lateral direction [25–27]. For both Au 90 and CNH nanoparticles which are spherical in nature, the manipulation can involve rolling, sliding, and rotation about the vertical axis [38]. In the case of the MoS_2 and WS_2 nanotubes, manipulation can involve rolling, sliding, as well as in-plane rotation which occurs at a pivot point. This can happen when the nanotubes are not pushed directly at the center of its length. Similar observations were found for manipulations of carbon nanotubes on mica and graphite [13].

Figure 10.4 shows the friction forces during nanoparticle manipulation for Au 30 and Au 90 nanoparticles under dry and submerged-in-water conditions [25]. Here scale effects on friction and wear are of interest. The data shows that Au 90 exhibit higher friction forces compared to Au 30. As discussed by Maharaj and Bhushan [25], the normal load acting on the nanoparticle is due only to the mass of the nanoparticle since it is pushed from the side and the friction force is the result of adhesion between the nanoparticle and the silicon substrate. The adhesive force can include van der Waals forces under both dry and submerged-in-water conditions and meniscus forces under dry conditions. In this regime the friction force is not proportional to the normal load since it is dependent on the contact area. The friction force in this case, for single-nanoparticle contact of spherical shapes is proportional to $(\text{normal load})^{2/3}$ [4, 30, 37, 46]. The normal load comprises the external normal load and the adhesive force. Since the adhesive force is dependent on surface area, it is expected that the larger Au 90 nanoparticles will have a higher friction force compared to the smaller Au 30 nanoparticles and this is confirmed from the results shown in Fig. 10.4a, b for both dry and submerged-in-water conditions.

Figure 10.4b presents the result of measurements of the average friction force for Au 30 and Au 90 nanoparticles submerged in water. A normal load of 1 nN was

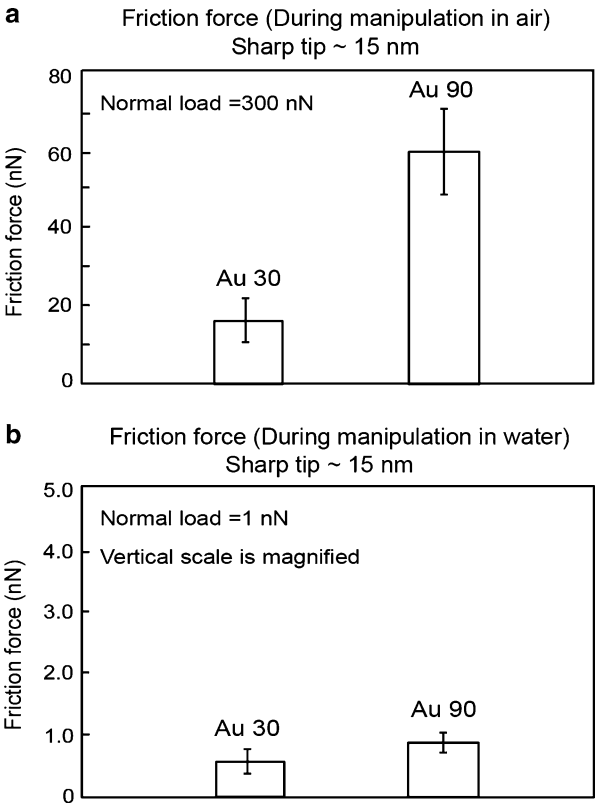

Fig. 10.4 Friction force for Au 30 and Au 90 nanoparticles on the silicon substrate during manipulation, at normal loads of (**a**) 300 nN in air and (**b**) 1 nN in water. The vertical scale has been magnified for data in water (Adapted from Maharaj and Bhushan [25])

used during manipulation as partial images cannot be obtained at higher load. This is sufficient since the nanoparticles are weakly adhered to the substrate and can be easily moved during the manipulation process and is discussed in further detail by Maharaj and Bhushan [25]. The adhesive forces are due to van der Waals interactions since there are no meniscus bridges formed under submerged-in-water conditions. The lower friction forces in the submerged-in-water condition compared to the dry condition can thus be attributed to the elimination of meniscus forces and sliding on a surface of low shear strength.

Figure 10.5 presents the results for the average friction forces for Au 90 and CNH nanoparticles and MoS_2 and WS_2 nanotubes under dry and submerged-in-liquid environments [26, 27]. Here material effects on friction and wear are of interest.

The friction force data for the nanoparticles and nanotubes in dry conditions are shown in Fig. 10.5a. There is an overall trend towards lower friction forces for the CNH nanoparticles and MoS_2 and WS_2 nanotubes compared to Au 90 nanoparticles. In the case of the nanotubes, it is not believed that exfoliation and tribofilm formation are responsible for the lower values as discussed by Maharaj and Bhushan [26, 27]. Here the nanotubes are pushed from the side, and there is no external pressure acting on the nanotubes to cause them to exfoliate.

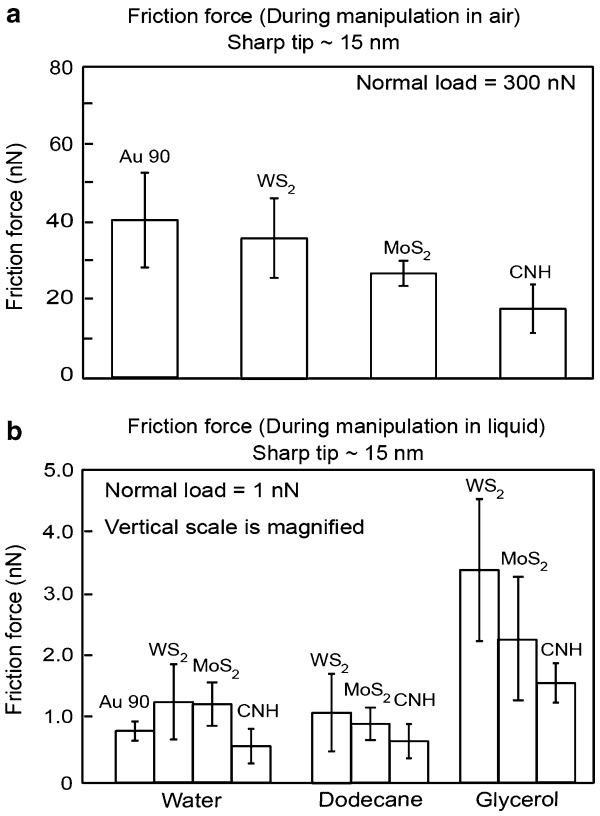

Fig. 10.5 Friction force for Au 90 and CNH nanoparticles and MoS_2 and WS_2 nanotubes on the silicon substrate during manipulation, at normal loads of (**a**) 300 nN in air and (**b**) 1 nN in liquids. The vertical scale is magnified for data in liquids [27]

The higher friction force observed for the Au 90 nanoparticles is due to attractive (adhesive) meniscus forces from water vapor in the atmosphere that condenses around the contact area of the nanoparticles and silicon substrate. As discussed by Maharaj and Bhushan [27], these attractive forces are larger on materials with higher work of adhesion (W_a). Table 10.1 gives the work of adhesion for thin films of Au, MoS_2 and WS_2, and graphene with their corresponding contact angles. W_a is calculated from the Dupré equation, given as

$$W_a = \gamma_l(1 + \cos\theta) \tag{10.1}$$

In this equation, γ_l is the surface tension or free surface energy of a liquid which is the additional energy available at the surface of the liquid due to fewer bonds with neighboring atoms and molecules [3]. A value of 72 mN/m at 25 °C is used for water [23] in this calculation. The static water contact angle, θ, is the angle between the water droplet and the substrate surface [3]. Higher work of adhesion means more work has to be done to separate the solid–liquid interface which contributes to greater attractive meniscus forces [3]. The work of adhesion is highest with Au films and lowest with graphene films. It is expected that since Au 90 nanoparticles

Table 10.1 Work of adhesion for thin films of Au, MoS_2, WS_2, and graphene in contact with water

Films	Water contact angle, θ (°)	Work of adhesion, W_a (mN/m^2)
Au	50[a]	118
MoS_2	75[b]	91
WS_2	93[c]	68
Graphene	127[d]	29

[a]Cayre and Paunov [8]
[b]Fuerstenau and Han [47]
[c]Zhang et al. [44]
[d]Wang et al. [42]

will have a higher work of adhesion compared to CNH nanoparticles and MoS_2 and WS_2 nanotubes, the meniscus force contribution to adhesion will be greater. This increased adhesion accounts for the higher friction force observed with the Au 90 nanoparticles. For the CNH nanoparticles, it is believed that the reduced contact area, due to the roughness provided by the nanohorns and the reduced meniscus force contribution, is responsible for the lowest observed friction forces [27].

Figure 10.5b presents the friction forces for the nanoparticles and nanotubes submerged-in-liquid conditions. In liquids, the adhesive forces are due to van der Waals interactions since there are no meniscus bridges being formed under the submerged-in-liquid condition. The lower friction forces under the submerged-in-liquid conditions compared to the dry conditions can be attributed to the elimination of meniscus forces and nanoparticles and nanotubes sliding on a low shear strength surface. Similar to dry conditions, exfoliation of MoS_2 and WS_2 nanotubes does not occur, and there is no contribution from tribofilm formation. The lowest friction forces occur with the CNH nanoparticles due to the low contact area provided by the roughness of the nanohorns. The highest friction force occurs in glycerol, which has the highest viscosity of the liquids used and therefore the greatest contribution to viscous drag force. Even though dodecane has a greater viscosity than water, it is still not sufficiently high enough to give a significant contribution to drag forces on the nano-objects or the AFM tip, which explains the similarity in friction forces observed for both liquids with and without nanoparticles and nanotubes.

Multiple-Nano-object Contact Sliding of a Glass Sphere over Several Nano-objects in Dry and Submerged-in-Liquid Conditions

Nanoscale Friction

In multiple-nano-object contact, the effect of the normal load acting on the nanoparticles and nanotubes between two surfaces was studied to determine the effects on the friction force. Figure 10.6 summarizes the coefficient of friction under dry and submerged-in-water conditions for Au 30 and Au 90. Here scale effects on friction and wear are of interest. Maharaj and Bhushan [25] showed that the coefficients of friction were lower for sliding under submerged-in-water

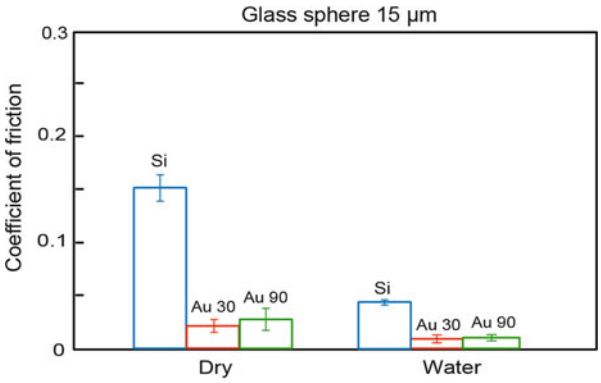

Fig. 10.6 Coefficients of friction for both dry and water conditions, with and without Au particles. Friction forces are lower for sliding on nano-objects in all conditions with lowest values obtained in water conditions (Adapted from Maharaj and Bhushan [25])

conditions as compared to sliding in dry conditions for both nano-object-coated and uncoated surfaces. The coefficient of friction is also lower for sliding on Au 30 nanoparticles compared to Au 90. This is expected since the lateral manipulation of the nanoparticles resulted in lower friction forces for Au 30 nanoparticles compared to Au 90. The difference is more pronounced under the dry conditions compared to sliding under water conditions. This occurs since, under the submerged conditions, the nanoparticles and cantilever are completely covered by water, and the meniscus force contribution to the friction force is eliminated. One must also consider that, since the glass sphere is glued to the cantilever, the addition of the epoxy could contribute to an increased stiffness (k) of the cantilever, making it less sensitive to detecting changes in the lateral friction force signal, especially for sliding in water where friction force signals are lower [25].

It has also been demonstrated that sliding on multiple asperities on nanopatterned surfaces [7] results in the reduction of friction. In this particular case, the asperities are immobile, and reduction occurs as a result of the reduced contact area. For sliding on Au nanoparticles, coefficient of friction reduction can be attributed to the mobility of the nanoparticles in addition to the reduced contact area. It is expected that as the glass sphere comes into contact with the Au nanoparticles, some of them will be deformed, since the larger nanoparticles will be encountered first and experience the highest contact pressures, due to fewer particles supporting the normal load. The resulting friction reduction mechanism can thus be attributed to the reduced contact area, the sliding over deformed nanoparticles, and individual nanoparticles sliding with the glass sphere. It is also possible for some rolling to take place as the sphere encounters a greater number of nanoparticles, and the contact pressure is reduced, leading to undeformed nanoparticles which may roll between the surface. In addition to elimination of meniscus forces, the presence of a liquid film between the glass sphere and the silicon substrate provides a low shear strength interface [6] which also contributes to the reduction in the coefficient of friction.

Figure 10.7 summarizes the coefficient of friction for Au 90 and CNH nanoparticles and MoS_2 and WS_2 nanotubes in dry and submerged-in-liquid conditions [26, 27]. Here material effects on friction and wear are of interest.

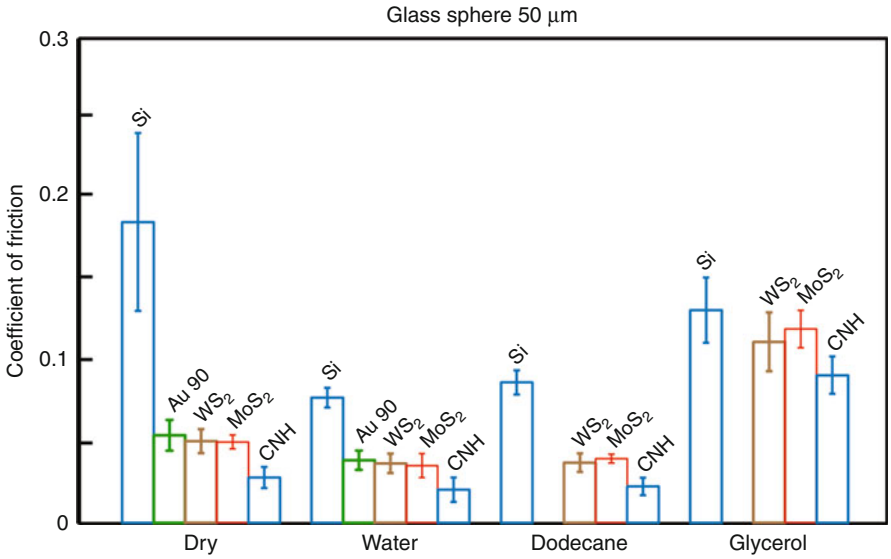

Fig. 10.7 Coefficients of friction for both dry and submerged-in-liquid conditions, with and without nano-objects. Friction forces are lower for sliding on nano-objects in all conditions with lowest values obtained in water conditions (Adapted from Maharaj and Bhushan [27])

In general, sliding on nano-objects results in lower coefficients of friction for all cases compared to sliding on the silicon substrate.

In dry conditions, the coefficient of friction data for the CNH nanoparticles and the MoS_2 and WS_2 nanotubes are generally lower than the Au 90 nanoparticles. As in the case of single-nano-object contact, with the Au 90 nanoparticle there is a higher meniscus force contribution to friction compared to the CNH nanoparticles and MoS_2 and WS_2 nanotubes. Exfoliation and tribofilm formation of the nanotubes, as shown in Fig. 10.2d, e, are not believed to occur due to the low contact pressure as discussed by Maharaj and Bhushan [26, 27]. This is evident in the similar coefficients of friction obtained for the Au 90 nanoparticles and MoS_2 and WS_2 nanotubes under dry and water conditions.

In macroscale experiments (not shown) using a ball-on-flat tribometer, Maharaj and Bhushan [27] slid a sapphire sphere over nanoparticle and nanotube-coated and uncoated silicon substrates for 500 cycles under a normal load of 200 mN in dry conditions. In these experiments MoS_2 and WS_2 nanotubes exhibited lower coefficients of friction compared to Au 90 with the lowest coefficient of friction observed with CNH nanoparticles. SEM micrographs taken of the wear scars showed crushed MoS_2 and WS_2 nanotubes which occurs due to the high contact pressure, and this is believed to be responsible for some exfoliation and tribofilm formation in dry conditions. The tribofilm provides a low shear strength surface for sliding and contributes to lower friction. With the CNH nanoparticles, the reduced contact area, as a result of the roughness of the nanohorns, and low meniscus force contribution are responsible for the low friction forces.

In submerged-in-liquid conditions, the coefficients of friction were lower compared to dry conditions. For water, as the meniscus forces are eliminated, the coefficient of friction data shows very little difference for Au 90 nanoparticles and MoS_2 and WS_2 nanotubes. The CNH nanoparticles have the lowest coefficient of friction in all liquid conditions due to the reduced contact area. The highest friction force and coefficient of friction occurs in glycerol, which has the highest viscosity and therefore results in a greater contribution from viscous drag force similar to single-nano-object contact followed by dodecane. The elimination of the meniscus forces together with sliding on surface of low shear strength as mentioned earlier results in lower coefficients of friction compared to dry conditions.

Nanoscale Wear

For a potential lubricant to be considered effective, it must not only be able to reduce the coefficient of friction, but also protect the underlying surface. Figure 10.8 summarizes the wear data for sliding on Si and Si coated with Au 90 and CNH nanoparticles and MoS_2 and WS_2 nanotubes [26, 27]. Typical wear data for nanoparticles are shown for 1, 10, and 100 cycles at a normal load of 20 μN under dry conditions, using CNH as an example. Wear data for Si and all nanoparticles and nanotubes are shown for 100 cycles in Fig. 10.8b. A 20 × 20 μm area is imaged to show wear scars which were created over a 10 × 10 μm area. Topography maps along with corresponding height profiles are also shown.

After 1 cycle the CNH nanoparticles are just beginning to be pushed out of the wear area. After 10 cycles the CNH nanoparticles are pushed out of the wear area and agglomerate around the edges of the wear scar. Similar observations were made for the other nano-objects for 1 and 10 cycles and are not shown here. For the uncoated silicon substrate after 100 cycles, a small amount of material is removed with a wear depth of approximately 0.25 nm as seen in the height profile. For the coated surfaces, very few nanoparticles and nanotubes remain in the wear area for MoS_2 and WS_2 nanotubes, while for CNH and Au 90 nanoparticles, they are completely removed after 100 cycles.

Figure 10.9 shows SEM micrographs of the wear scars in dry conditions (first row) after 100 cycles [26, 27]. Magnified micrographs of the areas within the squares are shown in the second row as indicated by the vertical arrows. In the magnified micrographs, agglomerated Au 90 and CNH nanoparticles and broken MoS_2 and WS_2 nanotubes are pointed out by arrows within each micrograph. Agglomeration and breaking of the nanoparticles and nanotubes can occur during the wear process. In the case of the MoS_2 and WS_2, broken nanotubes can also result, while samples are being prepared during sonication as they collide with one another. Since there is no evidence for crushed nanotubes from the SEM micrographs, it is unlikely that exfoliation of MoS_2 and WS_2 nanotubes would occur. It is not expected that there would be protection of the substrate from wear due to tribofilm formation.

It is believed, since the nanoparticles and nanotubes remain in the wear area after 1 cycle, that the damage of the silicon surface should be less than that of an initially uncoated substrate. This occurs since the nanoparticles and nanotubes are believed

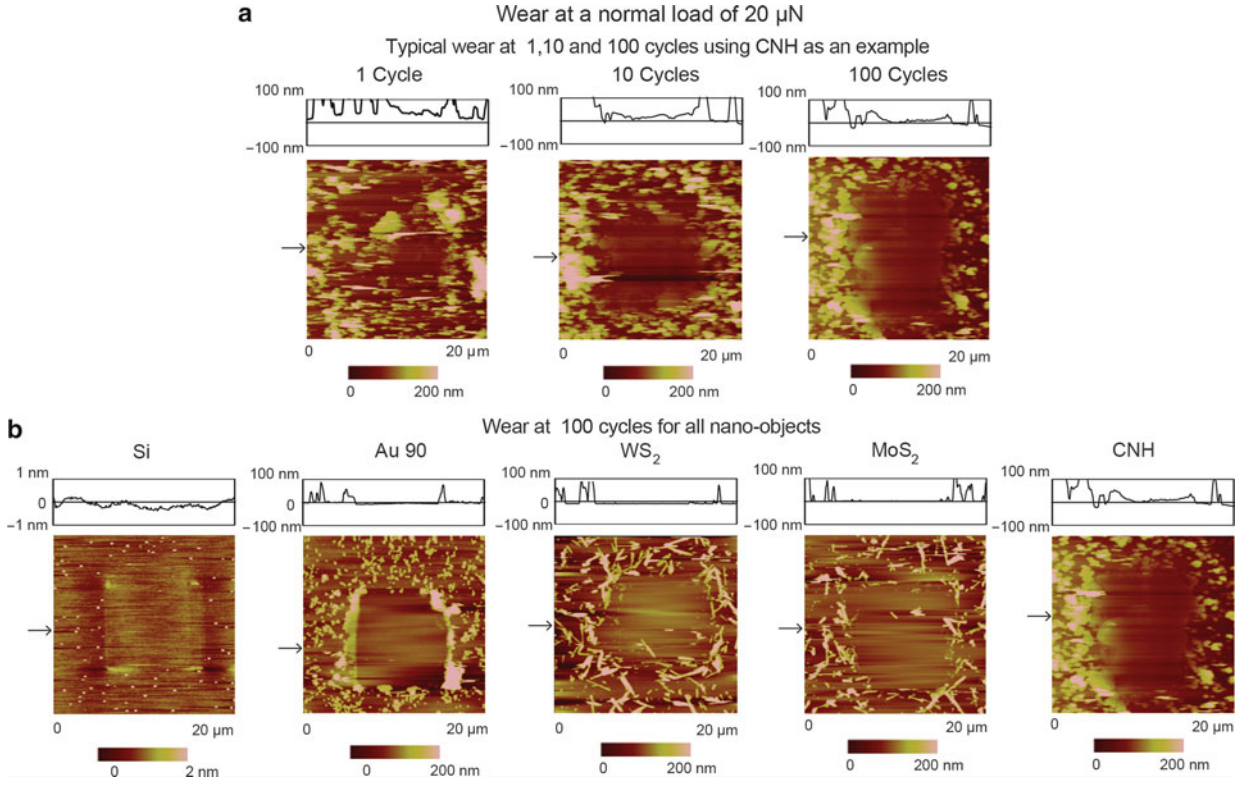

Fig. 10.8 Topography maps and 2D profiles, at sections shown by the *arrows*, after sliding at 1, 10, and 100 cycles with CNH at a normal load of 20 μN on Si and Si coated with CNH nanoparticles as an example (*first row*). Topography maps and 2D profiles, at sections shown by the *arrows*, after sliding at 100 cycles for Si and Si coated with Au and CNH nanoparticles and MoS_2 and WS_2 nanotubes (*second row*) (Adapted from Maharaj and Bhushan [27])

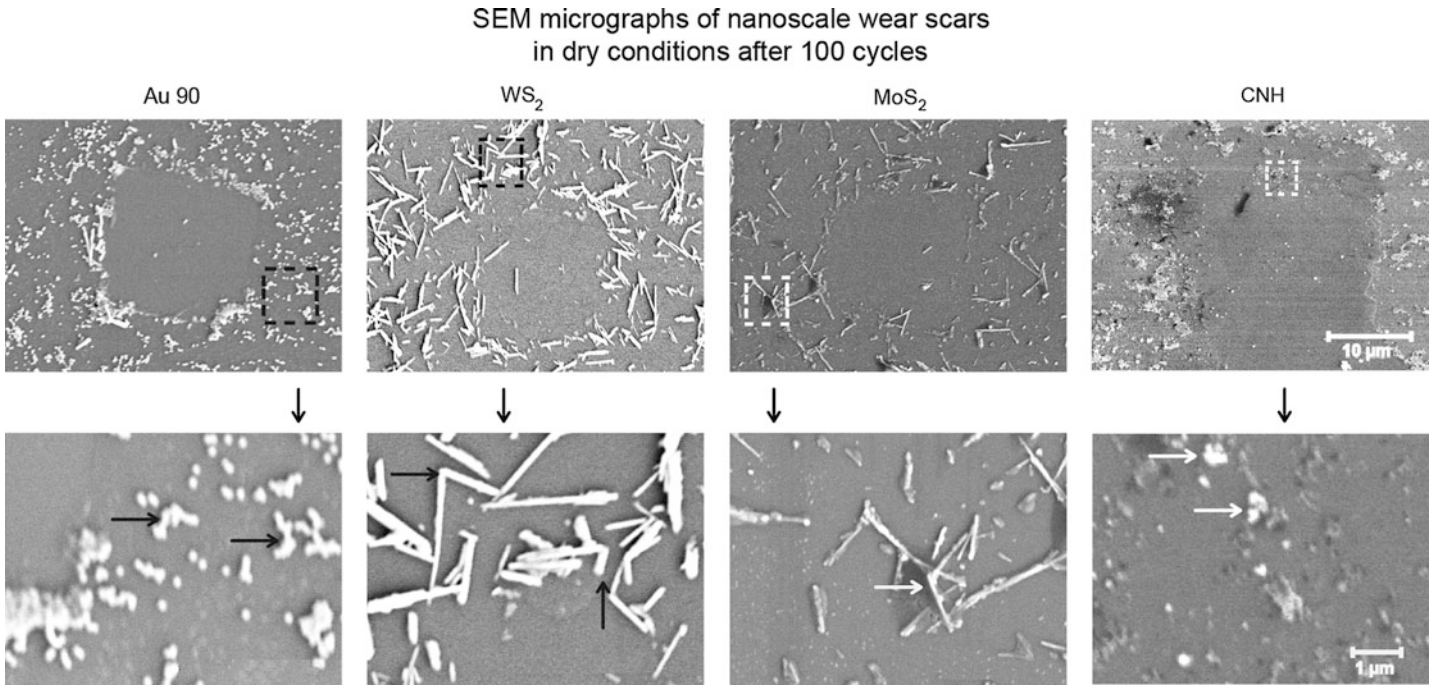

Fig. 10.9 SEM micrographs of nanoscale wear scars for Au 90 and CNH nanoparticles and MoS_2 and WS_2 nanotubes in dry conditions after 100 cycles at a normal load of 20 µN (*first row*). The nano-objects within the squares are magnified and the *vertical arrows* point to those micrographs in the *second row*. The magnified micrographs show agglomerated Au 90 and CNH nanoparticles and broken MoS_2 and WS_2 nanotubes as indicated by *arrows* within the micrographs [27]

to roll and slide between the glass sphere and the substrate which promotes facile shearing of the two surfaces, in addition to the reduced contact area provided by the nano-objects. For the CNH nanoparticles, the reduction in contact area due to the roughness provided by the nanohorns is expected to further reduce wear. After 100 cycles, it is therefore expected that the greatest wear occurs on the bare silicon substrate and the presence of nanoparticles and nanotubes does provide protection of the substrate with the least wear occurring with the CNH nanoparticles.

Conclusions

In this chapter an overview of friction and wear on the nanoscale was presented. Au and carbon nanohorn (CNH) nanoparticles and MoS_2 and WS_2 nanotubes have been investigated for their effect on friction and wear in dry and liquid conditions in water, dodecane, and glycerol. Studies presented were conducted in both single- and multiple-nano-object contacts with the aid of an AFM. For single-nanoparticle contact, when scale effects were compared, it was shown that friction force was greater for Au 90 compared to Au 30 in both dry and submerged-in-water conditions. When material effects were compared, the lowest friction forces were obtained with the CNH nanoparticles compared to Au nanoparticles and MoS_2 and WS_2 nanotubes. This is due to the reduced contact area provided by the roughness of the nanohorns and low meniscus force contribution in dry conditions. Lower friction forces occur in submerged-in-liquid conditions compared to dry conditions due to elimination of meniscus force and sliding on a low shear strength surface among the various liquids. The highest friction forces occur in glycerol due to high viscosity.

For multiple-nano-object contact, sliding over nanoparticles and nanotubes reduced coefficients of friction compared to sliding on the bare silicon substrate due to reduced contact area and rolling and sliding among the various nanoparticles and nanotubes in dry conditions. Similar scale effects were observed as in single-nano-object contact with Au nanoparticles. When material effects were compared, the lowest coefficient of friction occurs with the CNH nanoparticles compared to the other nano-objects due to the mechanisms mentioned for single-nano-object contact in dry conditions. In liquid conditions the coefficient of friction was lower compared to dry conditions due to the mechanisms mentioned for single-nano-object contact. In nanoscale wear experiments in dry conditions, the addition of nanoparticles and nanotubes prevents the glass sphere from coming directly into contact with the surface and reduces the wear of the substrate through possible rolling and sliding of the nanoparticles and nanotubes.

In macroscale studies (not shown), sliding over the various nanoparticles and nanotubes reduced friction and wear due to the mechanisms mentioned in multiple-nano-object contact on the nanoscale. Additionally, in dry conditions, sliding on the nanotubes reduced the coefficient of friction and the wear due to exfoliation and tribofilm formation.

In this chapter studies on nanomanipulation of nanoparticles and nanotubes in dry and liquid environments to determine friction forces have been presented and will aid in better design of applications requiring controlled manipulation and targeting of nanoparticles and nanotubes. Nanotribological studies have been presented and demonstrate the ability of nanoparticles and nanotubes to reduce friction and wear in dry and liquid environments.

References

1. Akbulut M, Belman N, Golan Y, Israelachvili JN (2006) Frictional properties of confined nanorods. Adv Mater 18:2589–2592
2. Berlin JM, Yu J, Lu W, Walsh EE, Zhang L, Zhang P, Chen W, Kan AT, Wong MS, Tomson MB, Tour JM (2011) Engineered nanoparticles for hydrocarbon detection in oil-field rocks. Energy Environ Sci 4:505–509
3. Bhushan B (ed) (2010) Springer handbook of nanotechnology, 3rd edn. Springer, Heidelberg
4. Bhushan B (ed) (2011) Nanotribology and nanomechanics, I and II, 3rd edn. Springer, Heidelberg
5. Bhushan B, Gupta BK (1991) Handbook of tribology: materials, coatings, and surface treatments. McGraw-Hill, New York
6. Bhushan B, Sundararajan S (1998) Micro/nanoscale friction and wear mechanisms of thin films using atomic force and friction force microscopy. Acta Mater 46:3793–3804
7. Burton Z, Bhushan B (2005) Hydrophobicity, adhesion and friction properties of nanopatterned polymers and scale dependence for MEMS/NEMS. Nano Lett 5:1607–1613
8. Cayre OJ, Paunov VN (2004) Contact angles of colloid silica and gold particles at air–water and oil–water interfaces determined with the gel trapping technique. Langmuir 20:9594–9599
9. Cizaire L, Vacher B, Mogne T, Le Martin JM, Rapoport L, Margolin A, Tenne R (2002) Mechanisms of ultra-low friction by hollow inorganic fullerene-like MoS_2 nanoparticles. Surf Coat Technol 160:282–287
10. St Dennis JE, Jin K, John VT, Pesika NS (2011) Carbon microspheres as ball bearings in aqueous-based lubrication. ACS Appl Mater Interfaces 3:2215–2218
11. Dietzel D, Monninghoff GS, Jansen L, Fuchs H, Ritter C, Scharwz UD, Schirmeisen A (2007) Interfacial friction obtained by lateral manipulation of nanoparticles using atomic force microscopy techniques. J Appl Phys 102:084306
12. Duncan R (2003) The dawning era of polymer therapeutics. Nat Rev Drug Discov 2:347–360
13. Falvo MR, Taylor RM II, Helser A, Chi V, Brooks FP Jr, Washburn S, Superfine R (1999) Nanometre-scale rolling and sliding of carbon nanotubes. Nature 397:236–238
14. Ferrari M (2005) Cancer nanotechnology: opportunities and challenges. Nat Rev Cancer 5:161–171
15. Gourdon D, Yasa M, Godfrey Alig AR, Li Y, Safinya CR, Israelachvili JN (2004) Mechanical and structural properties of $BaCrO_4$ nanorod films under confinement and shear. Adv Funct Mater 14:238–242
16. Greenberg R, Halperin G, Etsion I, Tenne R (2004) The effect of WS_2 nanoparticles on friction reduction in various lubrication regimes. Tribol Lett 17:179–186
17. Hu HS, Dong JX, Chen GX (1998) Study on antiwear and reducing friction additive of nanometer ferric oxide. Tribol Int 31:355–360
18. Hui X, Regnier S (2012) High-efficiency automated nanomanipulation with parallel imaging/manipulation force microscopy. IEEE Trans Nanotechnol 11:21–33
19. Irvine DJ (2011) Drug delivery: one nanoparticle, one kill. Nat Mater 10:342–343
20. Joly-Pottuz L, Dassenoy F, Belin M, Vacher B, Martin JM, Fleischer N (2005) Ultralow-friction and wear properties of IF-WS_2 under boundary lubrication. Tribol Lett 18:477–485

21. Kalin M, Kogovšek J, Remškar M (2012) Mechanisms and improvements in the friction and wear behavior using MoS_2 nanotubes as potential oil additives. Wear 280–281:36–45
22. Lahouij I, Dassenoy F, de Knoop L, Martin J-M, Vacher B (2011) In situ TEM observation of the behavior of an individual fullerene-like MoS_2 nanoparticle in a dynamic contact. Tribol Lett 42:133–140
23. Lide DR (ed) (2009) CRC handbook of chemistry and physics, 90th edn. CRC Press, Boca Raton
24. Lüthi R, Meyer E, Haefke H, Howald L, Gutmannsbauer W, Güntherodt H-J (1994) Sled-type motion on the nanometer scale: determination of dissipation and cohesive energies of C60. Science 266:1979–1981
25. Maharaj D, Bhushan B (2012) Effect of spherical Au nanoparticles on nanofriction and wear reduction in dry and liquid environments. Beilstein J Nanotechnol 3:759–772
26. Maharaj D, Bhushan B (2013) Effect of MoS_2 and WS_2 nanotubes on nanofriction and wear reduction in dry and liquid environments. Tribol Lett 49:323–339
27. Maharaj D, Bhushan B (2013) Effect of carbon nanohorns on nanofriction and wear reduction in dry and liquid environments. J Colloid Interface Sci 400:147–160
28. Matteo C, Candido P, Vera R, Francesca V (2012) Current and future nanotech applications in the oil industry. Am J Appl Sci 9:784–793
29. Mougin K, Gnecco E, Rao A, Cuberes MT, Jayaraman S, McFarland EW, Haidara H, Meyer E (2008) Manipulation of gold nanoparticles: influence of surface chemistry, temperature, and environment (vacuum versus ambient atmosphere). Langmuir 24:1577–1581
30. Palacio M, Bhushan B (2008) A nanoscale friction investigation during manipulation of nanoparticles in controlled environments. Nanotechnology 19:315710
31. Panyala NR, Pena-Mendez EM, Havel J (2009) Gold and nano-gold in medicine: overview, toxicology and perspectives. J Appl Biomed 7:75–91
32. Rapoport L, Lvovsky M, Lapsker I, Leshinsky V, Volovik Y, Feldman Y, Zak A, Tenne R (2001) Slow release of fullerene-like WS_2 nanoparticles as a superior solid lubrication mechanism in composite matrices. Adv Eng Mater 3:71–75
33. Rapoport L, Nepomnyashchy O, Lapsker I, Verdyan A, Soifer Y, Popovitz-Biro R, Tenne R (2005) Friction and wear of fullerene-like WS_2 under severe contact conditions: friction of ceramic materials. Tribol Lett 19:143–149
34. Resch R, Lewis D, Meltzer S, Montoya N, Koel BE, Madhukar A, Requicha AA, Will P (2000) Manipulation of gold nanoparticles in liquid environments using scanning force microscopy. Ultramicroscopy 82:135–139
35. Ritter C, Heyde M, Stegemann B, Rademann K, Schwarz UD (2005) Contact-area dependence of frictional forces: moving adsorbed antimony nanoparticles. Phys Rev B 71:085405
36. Ryoo S, Rahmani AR, Yoon KY, Prodanovic M, Kotsmar C, Milner TE, Huh C (2012) Theoretical and experimental investigation of the motion of multiphase fluids containing paramagnetic nanoparticles in porous media. J Petrol Sci Eng 81:129–144
37. Schwarz UD, Zwörner O, Köster P, Wiesendanger R (1997) Quantitative analysis of the frictional properties of solid materials at low loads. I. Carbon compounds. Phys Rev B 56:6987–6996
38. Sitti M (2004) Atomic force microscope probe based controlled pushing for nanotribological characterization. IEEE/ASME Trans Mechatron 9:343–349
39. Tanaka A, Umeda K, Yudasaka M, Suzuki M, Ohana T, Yumura M, Iijima S (2005) Friction and wear of carbon nanohorn-containing polyimide composites. Tribol Lett 19:135–142
40. Tevet O, Von-Huth P, Popovitz-Biro R, Rosentsveig R, Wagner HD, Tenne R (2011) Friction mechanism of individual multilayered nanoparticles. Proc Natl Acad Sci U S A 108:19901–19906

41. Thanikaivelan P, Narayanan NT, Pradhan BK, Ajayan PM (2012) Collagen based magnetic nanocomposites for oil removal applications. Sci Rep 2:230. doi:10.1038/srep00230
42. Wang S, Zhang Y, Abidi N, Cabrales L (2009) Wettability and surface free energy of graphene films. Langmuir 25:11078–11081
43. Zhang J, Zhang J (2013) Surfactant inducing phase change of ZnO nanorods to low friction. Tribo Lett 49:77–83
44. Zhang S, Zeng XT, Tang ZG, Tan MJ (2002) Exploring the antisticking properties of solid lubricant thin films in transfer molding. Int J Mod Phys B 16:1080–1085
45. Singh DP, Polychronopoulou K, Rebholz C, Aouadi SM (2010) Room temperature synthesis and high temperature frictional study of silver vanadate nanorods. Nanotechnology 21:325601
46. Bhushan B (2013) Introduction to tribology, 2nd ed. Wiley, New York
47. Fuerstenau MC, Han KN (ed) (2003) Principles of mineral processing, society for mining, metallurgy, and exploration (SME). Littleton, Colorado